Determining systemic QSO redshifts from Mg II in the absence of narrow forbidden lines

David Gross*, David Tytler, David Kirkman, Jeffrey Lee, Aaron Day, Cameron Leung
Center for Astrophysics and Space Sciences, University of California San Diego, La Jolla, CA, 92093-0424

13 September 2011

ABSTRACT

We report the findings of a detailed investigation into the velocity shifts between the Mg II, [O II], and [O III] emission lines in a large sample of SDSS QSO spectra. Many methods of analysis are sensitive to the adopted redshift for each QSO. We aim to measure a precise systemic QSO redshift if we have a well-behaved Mg II emission peak in the observed frame with minimal absorption, but no narrow forbidden lines available for comparison. These findings are particularly useful for high-redshift QSOs without infrared spectra that can be used to measure [O II] or [O III].

Key words: quasars: emission lines – quasars: general – cosmology: observations

1 INTRODUCTION

In optical QSO spectra it is known that the redshifts of the forbidden lines are comparable to those of the low ionization lines. These two closely related groups occupy the narrow line region (NLR) where orbital speeds of the atomic clouds are relatively small compared to the more volatile broad line region (BLR). Because of the stability of the NLR, lines originating from it are often used to measure the systemic redshift of the QSO itself. The most commonly used lines for this task are the low-ionization forbidden lines [N II], [O II], [S II], and [O III]. The reliability of [O III] as an indicator for systemic redshift, however, has been seriously questioned in recent studies by Boroson (2005), Hewett (2010), and Zhang (2011). It is now known that the [O III] line is regularly asymmetric and blueshifted with respect to the systemic redshift by 40-45 km/s, with no dependence on the QSO luminosity (Boroson 2005, Hewett 2010). Accurate systemic redshifts are useful in a variety of QSO-related fields including clustering, outflows, and proximity effect determinations.

We seek to understand the situation where we need a precise systemic redshift for a high redshift ($0.8 \lesssim z \lesssim 2.2$) QSO when only an optical spectrum is available. In this situation the λ2798 Mg II line is most often observed, but the low ionization forbidden lines are partially or completely shifted off the optical plate. Ideally, we would like to make a precise measurement of the QSO's systemic redshift from Mg II alone without deferring to any low-ionization forbidden lines. In order to do this we must understand how physical properties of the Mg II, [O II], and [O III] lines correlate to specific line velocity shifts. In particular, we will investigate how an individual peak's broadening and width correlate to an observed velocity shift.

2 DATA SAMPLE

The complete SDSS DR5 quasar catalog is obtained (Schneider et. al. 2007). All spectra with a median signal-to-noise ratio in the R-band less than 15 as determined by the SDSS are discarded. In each spectrum, all unreliable pixels are masked based on the standard SDSS mask array values. We bring each spectrum into the rest frame using the SDSS determined redshift value.

We adopt the rest frame wavelengths of 2798.35 Å, 3728.30 Å, and 5008.24 Å, for Mg II,

* E-mail: dsgross@ucsd.edu

[O II], and [O III], respectively. For each peak, we investigate the region created by moving 180 Å, 30 Å, and 45 Å to the red and blue of the rest frame wavelength for Mg II, [O II], and [O III], respectively. If the defined region is not entirely observed, the spectrum is discarded.

A first-degree polynomial is fit to the defined peak region. To accomplish this, we first find the average flux density, μ and standard deviation of the average flux density, σ in this peak region. We then mask those pixels that have a flux density greater than $\mu + \frac{\sigma}{2}$. This provides a standard straight-line continuum fit to the local peak region.

The peak region is then split into three equal wavelength bins. In each bin, we measure the average deviation of the flux density from the local straight-line continuum fit. We then assume that the peak is located in the bin with the highest average deviation from the continuum fit. This works well for peaks with minimal absorption, which is what we're after, but a more complicated algorithm would have to be developed in the case of large self-absorption. The start and end wavelength of this bin define the limits for a skew normal distribution to be fit to the emission peak via the Levenberg-Marquardt algorithm.

The Mg II, [O II], and [O III] lines are fit with a skew normal distribution that generalizes the normal distribution to allow for non-zero skewness. This distribution is characterized by the real parameters: location ξ, scale ω, shape α, and height h with the probability distribution function:

$$pdf: he^{\frac{-(x-\xi)^2}{\omega^2}} \int_{-\infty}^{\alpha(\frac{x-\xi}{\omega})} e^{-t^2} dt$$

The broadening of any given emission line can be understood by the sign of the shape and scale parameters, as show in Table 1. The larger the value of $|\alpha|$ or $|\omega|$, the more respective broadening exists.

For each peak, the values of the rest location wavelength ξ, scale ω, shape α, height h, and continuum flux density are recorded. By understanding the skew normal distribution's pdf we are able to find the maximum of the distribution through a discrete iterative procedure. We consider the maximum of the distribution to be the true observed peak wavelength in the SDSS frame. The value of the continuum flux density is taken to be the value of the standard straight line continuum fit at the true observed peak wavelength in the SDSS frame. An example of this procedure as applied to a select Mg II, [O II], and [O III] peak is seen in Fig. 2.

In total, the fitting procedure was applied to 9443 Mg II peaks, 4159 [O II] peaks, and 3889 [O III] peaks. Mg II and [O II] were found in 1915 spectra, Mg II and [O III] were found in 1323 spectra, [O II] and [O III] were found in 2534 spectra, and Mg II, [O II], and [O III] were found in 679 spectra. The redshift and SNR distributions for the individual peaks are shown in Fig 1. The redshift and SNR distributions for various peak combinations are shown in Fig 2.

α	ω	Broadening Observed
+	+	Red
+	-	Blue
-	+	Red
-	-	Red

Table 1: Observed broadening for different combinations of the fitted shape and scale parameters

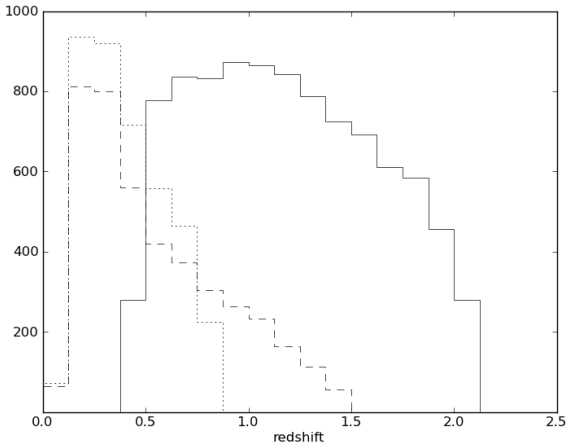

Figure 1.1: The redshift distribution of the fitted peaks. The solid line denotes Mg II, the dashed line denotes [O II], and the dotted line denotes [O III]. The average redshifts are 1.192 ± 0.005, 0.5546 ± 0.005, and 0.4102 ± 0.007 for Mg II, [O II], and [O III] respectively.

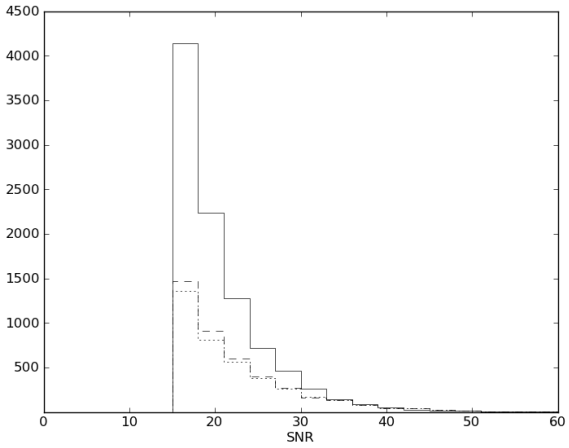

Figure 1.2: The SNR distribution of the fitted peaks. The solid line denotes Mg II, the dashed line denotes [O II], and the dotted line denotes [O III]. The average spectra SNRs are 20.39 ± 0.06, 22.07 ± 0.11, and 22.28 ± 0.12 for Mg II, [O II], and [O III] respectively.

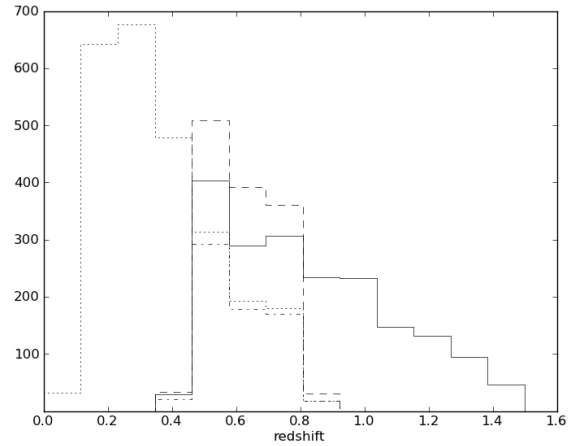

Figure 3.1: The redshift distribution of various peak combinations found in the spectra. The solid line denotes spectra where Mg II and [O II] were found, the dashed line denotes spectra Mg II and [O III] were found, the dotted line denotes spectra where [O II] and [O III] were found, and the dashed-dotted line denotes spectra where Mg II, [O II], and [O III] were found. The average spectra redshifts are 0.8231 ± 0.0060 for Mg II & [O II], 0.6213 ± 0.0029 for Mg II & [O III], 0.3707 ± 0.0036 for [O II] & [O III], and 0.6112 ± 0.0040 for Mg II, [O II], & [O III].

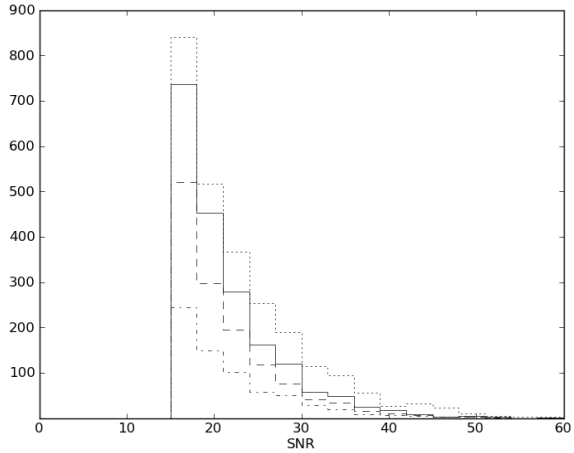

Figure 2.2: The SNR distribution of various peak combinations found in the spectra. The solid line denotes spectra where Mg II and [O II] were found, the dashed line denotes spectra where Mg II and [O III] were found, the dotted line denotes spectra where [O II] and [O III] were found, and the dashed-dotted line denotes spectra where Mg II, [O II], and [O III] were found. The average spectra SNRs are 21.72 ± 0.14 for Mg II & [O II], 21.16 ± 0.17 for Mg II & [O III], 22.67 ± 0.15 for [O II] & [O III], and 21.81 ± 0.26 for Mg II, [O II], & [O III].

3 RESULTS

3.1 THE SHAPE AND SCALE PARAMETERS

The scale parameter ω is plotted against the shape parameter α for each fitted line in Fig. 4. Any Mg II or [O III] peak can be characterized by one of the four distinct groupings shown. The [O II] peaks do not form the same distinctive groups because of their weaker relative strength. 5370 or 57.2% of the Mg II peaks show blue broadening, 2430 or 58.4% of the [O II] peaks show red broadening, and 2641 or 63.3% of the [O III] peaks show blue broadening. These are new results that finally quantify the broadening seen in Mg II and [O II] peaks and sheds light on the common asymmetry seen in [O III] peaks by Boroson and many others.

3.2 COMAPARISON TO SDSS-DERIVED REDSHIFT VALUES

The Mg II, [O II], and [O III] velocity shifts from the reported systemic SDSS redshift values

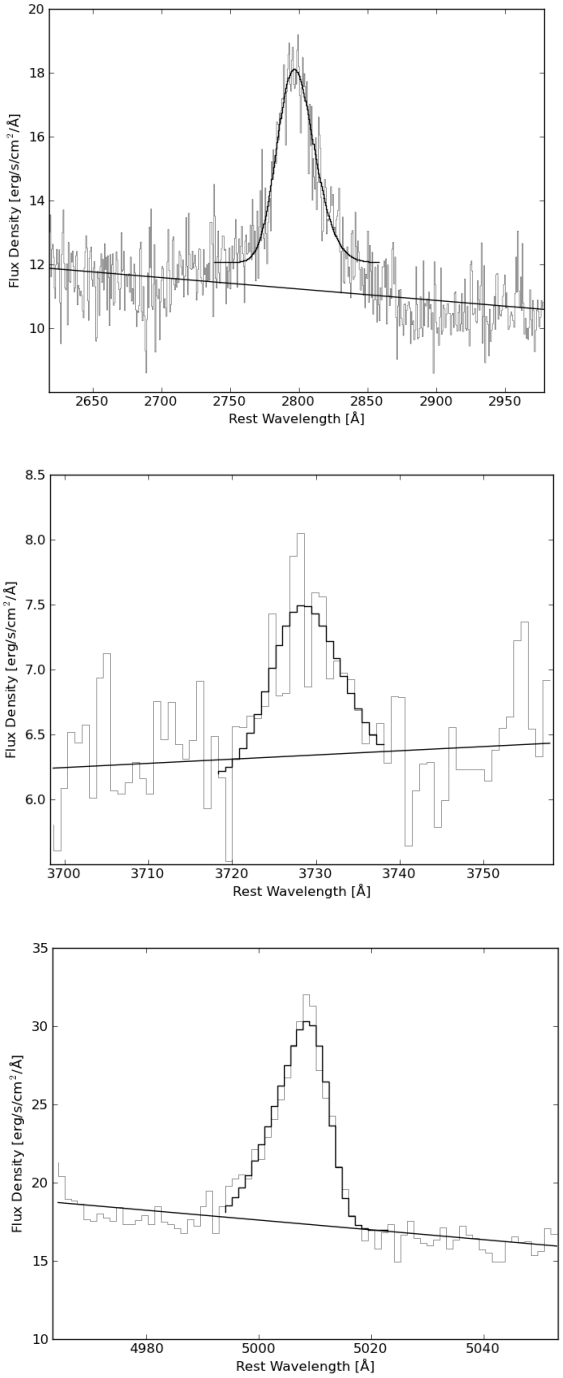

Figure 2: An example Mg II, [O II], and [O III] peak fit via the routine described. The straight solid line is the first-degree continuum fit. The other solid line is the skewed Gaussian fit to the peak. Note that the Gaussian fit is plotted with the same resolution of the data, but in actuality it is computed as a continuous nonanalytic function.

are shown in Fig. 5. We report average offsets of 361 $\pm$ 5 km/s, 61 $\pm$ 6 km/s, and 40 $\pm$ 2 km/s from the reported SDSS QSO systemic redshift value for Mg II, [O II], and [O III], respectively. The Mg II line shows the most spread with a standard deviation of 495 km/s, while the [O II] and [O III] lines hold truer to the reported SDSS redshift with standard deviations of only 359 km/s and 141 km/s, respectively. The Mg II line is shifted to the red of the SDSS redshift 81.2% of the time, while the [O II] and [O III] lines are shifted to the red 80.1% and 68.3% of the time, respectively. Among those Mg II peaks measured to the red of the SDSS systemic redshift, the average α is 0.83 $\pm$ 0.02 and the average ω is -15.2 $\pm$ 0.3. Among those Mg II peaks measured to be to the blue of the SDSS systemic redshift, the average α is -0.004 $\pm$ 0.04 and the average ω is -18.3 $\pm$ 0.7.

It is interesting that over the total sample we find a common and significant redshift of both [O II] and [O III] with respect to the SDSS systemic redshift. We expected that [O II] would be near the SDSS systemic redshift value (certainly $\pm$ 15-20 km/s) and that [O III] would be found at -45 km/s based on the results of Boroson (2005) and Hewett & Wild (2011). If we assume that our [O III] measurements are correct, it appears that in most cases the SDSS systemic redshift is too blue by some 60-80 km/s. Our findings could mean that the SDSS pipeline that assigns a systemic redshift to each targeted QSO via a weighted average of emission peak redshifts is inaccurate. It would be interesting to test our velocity shifts against the Princeton pipeline if more time was allowed as Hewett & Wild pointed out a significant discrepancy that grows with increasing redshift between the two pipelines last year. This does not explain the high offset to the red we measure in [O II], however. We comment that the [O II] line profile is also often asymmetric and not always well-defined in any given QSO spectrum. It seems reasonable that using different automated fitting methods or even a manual fitting method could return an inherent spread of 15-20 km/s. Our results suggest that [O II] averages to the red of the systemic redshift by 15-20 km/s which follows more closely to what Boroson found in 2005 rather than Hewett & Wild's finding of -20 km/s for the same measurement in 2011.

3.3 RELATIVE LINE VELOCITY RELATIONSHIPS

Being that all of the spectra are now in the SDSS frame, it is a simple procedure to make direct velocity comparisons between two or three lines to find their respective relative redshift(s). We do this for [O II] – [O III], [O III] – Mg II, and [O II] – Mg II in Fig. 6 and report average shifts of 64 $\pm$ 3 km/s, -76 $\pm$ 8 km/s, and -43 $\pm$ 7 km/s, respectively. These results are self-consistent and are in good agreement with previously published results as seen in Table 2.

Line Combination	Velocity Shift [km/s]	Group
Mg II – [O II]	-200 $\pm$170	Wilkes (1986)
Mg II – [O II]	380 $\pm$ 80	Junkkarinen (1989)
[O II] - [O III]	100 $\pm$ 130	Wilkes (1986)

Table 2: Previously published values for the line combinations under inspection.

These results further reinforce that using [O III] instead of [O II] or vice versa to measure the systemic redshift of a QSO will lead to significant discrepancies between precision groups, although both lines do originate from the NLR.

3.4 RELATIVE LINE VELOCITY RELATIONSHIPS – FURTHER INVESTIGATION AND COMPARSION TO SDSS

We now explain these velocity shifts in terms of the shape and scale parameters being investigated. For the α and ω parameter values shown in Fig.4 we find a new value β which represents the two parameters added together in quadrature for each peak such that:

$$\beta = \sqrt{\alpha^2 + \omega^2}$$

We find the average and standard deviation of β for all red and blue broadened Mg II, [O II], and [O III] peaks separately. Those β values that lay within $0 : \mu + \sigma$ form a “normal broadening” category. β values > $\mu + \sigma$ constitute “large broadening”.

These groupings are used to present each peak’s offset from the SDSS redshift more accurately in Table 3. For Mg II, an average range of 150-471 km/s is possible simply based on the broadening observed in the Mg II peak. This compares to 33-99 km/s seen for [O II] and 14-80 km/s seen for [O III]. Recall that our average Mg II offset from the SDSS reported redshift was found to be 361 $\pm$ 5 km/s. From Table 3, we can see that depending on the Mg II α and ω parameters this average shift can vary -211 to +110 km/s from the average value. The [O II] and [O III] peaks do not show as much spread with -30 to 38 km/s and -26 to 40 km/s, respectively. We note that there are no consistent peak-to-peak broadening trends; this adds supporting evidence to the notion of a dynamic NLR as Boroson suggests.

Mg II Category	Average Offset from SDSS Redshift [km/s]
Large Red Broadening	156 $\pm$ 6
Normal Red Broadening	237 $\pm$ 4
Large Blue Broadening	392 $\pm$ 13
Normal Blue Broadening	465 $\pm$ 6

[O II] Category	Average Offset from SDSS Redshift [km/s]
Large Red Broadening	49 $\pm$ 2
Normal Red Broadening	76 $\pm$ 2
Large Blue Broadening	93 $\pm$ 6
Normal Blue Broadening	37 $\pm$ 1

[O III] Category	Average Offset from SDSS Redshift [km/s]
Large Red Broadening	75 ± 5
Normal Red Broadening	15 ± 1
Large Blue Broadening	65 ± 3
Normal Blue Broadening	44 ± 1

Table 3: We can classify any given Mg II, [O II], or [O III] peak by its broadening and discuss the implications for its offset from the SDSS value.

We now do a similar analysis for all possible broadening combinations of [O II] – Mg II, [O III] – Mg II, and [O II] – [O III] in Table 4. We note a few interesting trends that are uncovered.

1. In the case of the large Mg II red broadening sample, the value of [O II] – Mg II increases as the [O II] peak tends toward bluer broadening. This is precisely the opposite action of the [O III] peak in the same Mg II sample as the value of [O III] – Mg II decreases with bluer [O III] broadening.
2. It appears that in general, as the Mg II peak exhibits redder broadening, the value of [O II] – Mg II increases.
3. It appears that in general, as the Mg II peak exhibits redder broadening, the value of [O III] – Mg II also increases.
4. It appears that in general, as the [O III] peak exhibits bluer broadening, the value of [O III] – [O II] decreases.
5. It appears that in general, as the [O II] peak exhibits redder broadening, the value of [O III] – [O II] decreases.

***MORE NEEDS TO BE EXPLAINED HERE / CARTOONS?* I'm going to need some help here.**

4 CONCLUSION

Based on this work, what statements can I make about the systemic redshift based solely on a measurement of Mg II? Should I quote 2σ values? I'm going to need some help here.

5 ACKNOWLEDGEMENTS

Funding for the creation and distribution of the SDSS Archive has been provided by the Alfred P. Sloan Foundation, the Participating Institutions, the National Aeronautics and Space Administration, the National Science Foundation, the Department of Energy, the Japanese Monbukagakusho, and the Max Planck Society. The SDSS Web site is http://www.sdss.org. The Participating Institutions in the SDSS are the University of Chicago, Fermilab, the Institute for Advanced Study, the Japan Participation Group, the Johns Hopkins University, the Max Planck Institute for Astronomy, the Max Planck Institute for Astrophysics, New Mexico State University, Princeton University, the United States Naval Observatory, and the University of Washington.

6 REFERENCES

Boroson, T., 2005, AJ, 130, 381

Carswell, R., 1991, AJ, 381, L5-L8

Hewett, P., Wild, V., 2010, MNRAS, 405, 2302

Richards, G. et. al., 2002, AJ, 124, 1

Schneider, D. et. al., 2007, AJ, 134, 102

Tytler, D., Fan, X., 1992, AJ, 79, 1

Zhang et. al., 2011, preprint.

First Peak Category	Second Peak Category	Second Peak Category – First Peak Category Average Velocity Shift [km/s]
Large Mg II Red Broadening	Large [O II] Red Broadening	31 ± 135
	Normal [O II] Red Broadening	200 ± 97
	Large [O II] Blue Broadening	699 ± 370
	Normal [O II] Blue Broadening	217 ± 140
	Large [O III] Red Broadening	350 ± 552
	Normal [O III] Red Broadening	89 ± 122
	Large [O III] Blue Broadening	-71 ± 33
	Normal [O III] Blue Broadening	2 ± 80
Normal Mg II Red Broadening	Large [O II] Red Broadening	-153 ±73
	Normal [O II] Red Broadening	26 ± 31
	Large [O II] Blue Broadening	-22 ± 55
	Normal [O II] Blue Broadening	-115 ± 38
	Large [O III] Red Broadening	31 ± 51
	Normal [O III] Red Broadening	-9 ± 43
	Large [O III] Blue Broadening	-52 ± 23
	Normal [O III] Blue Broadening	15 ± 33
Large Mg II Blue Broadening	Large [O II] Red Broadening	-142 ± 134
	Normal [O II] Red Broadening	-249 ± 79
	Large [O II] Blue Broadening	-79 ± 80
	Normal [O II] Blue Broadening	-389 ± 105
	Large [O III] Red Broadening	-30 ± 115
	Normal [O III] Red Broadening	17 ± 74
	Large [O III] Blue Broadening	-115 ± 67
	Normal [O III] Blue Broadening	-114 ± 45
Normal Mg II Blue Broadening	Large [O II] Red Broadening	-182 ± 48
	Normal [O II] Red Broadening	-149 ± 26
	Large [O II] Blue Broadening	-165 ± 68
	Normal [O II] Blue Broadening	-254 ± 45
	Large [O III] Red Broadening	-175 ± 38
	Normal [O III] Red Broadening	-137 ± 18
	Large [O III] Blue Broadening	-126 ± 19
	Normal [O III] Blue Broadening	-73 ± 27
Large [O II] Red Broadening	Large [O III] Red Broadening	78 ± 105
	Normal [O III] Red Broadening	-9 ± 67
	Large [O III] Blue Broadening	-66 ± 131
	Normal [O III] Blue Broadening	48 ± 33
Normal [O II] Red Broadening	Large [O III] Red Broadening	77 ± 40
	Normal [O III] Red Broadening	38 ± 13
	Large [O III] Blue Broadening	-8 ± 40
	Normal [O III] Blue Broadening	30 ± 8
Large [O II] Blue Broadening	Large [O III] Red Broadening	370 ± 113
	Normal [O III] Red Broadening	101 ± 23
	Large [O III] Blue Broadening	96 ± 86
	Normal [O III] Blue Broadening	100 ± 29
Normal [O II] Blue Broadening	Large [O III] Red Broadening	83 ± 50
	Normal [O III] Red Broadening	55 ± 8
	Large [O III] Blue Broadening	39 ± 47
	Normal [O III] Blue Broadening	42 ± 7

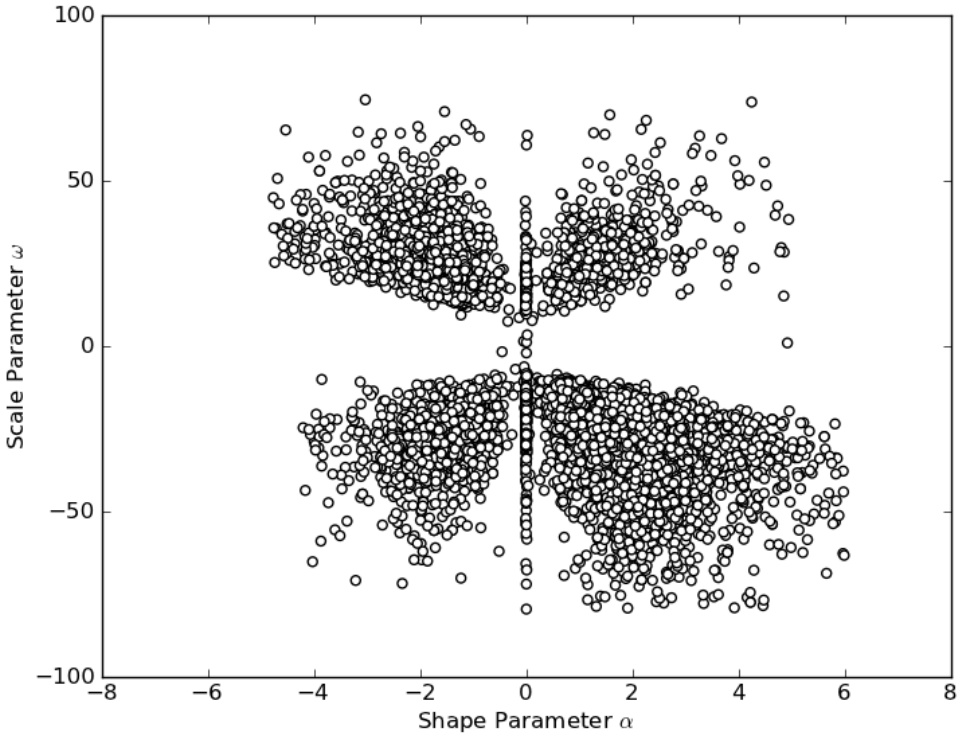

Figure 4.1: A scatterplot of the shape and scale parameters for the total Mg II sample.

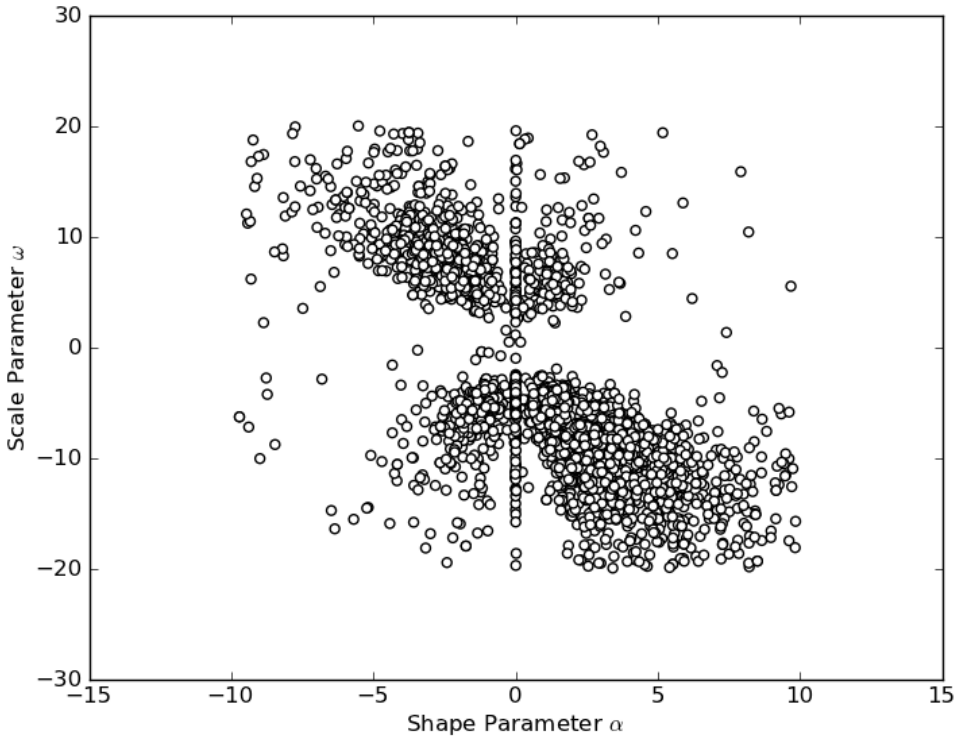

Figure 4.2: A scatterplot of the shape and scale parameters for the total [O II] sample.

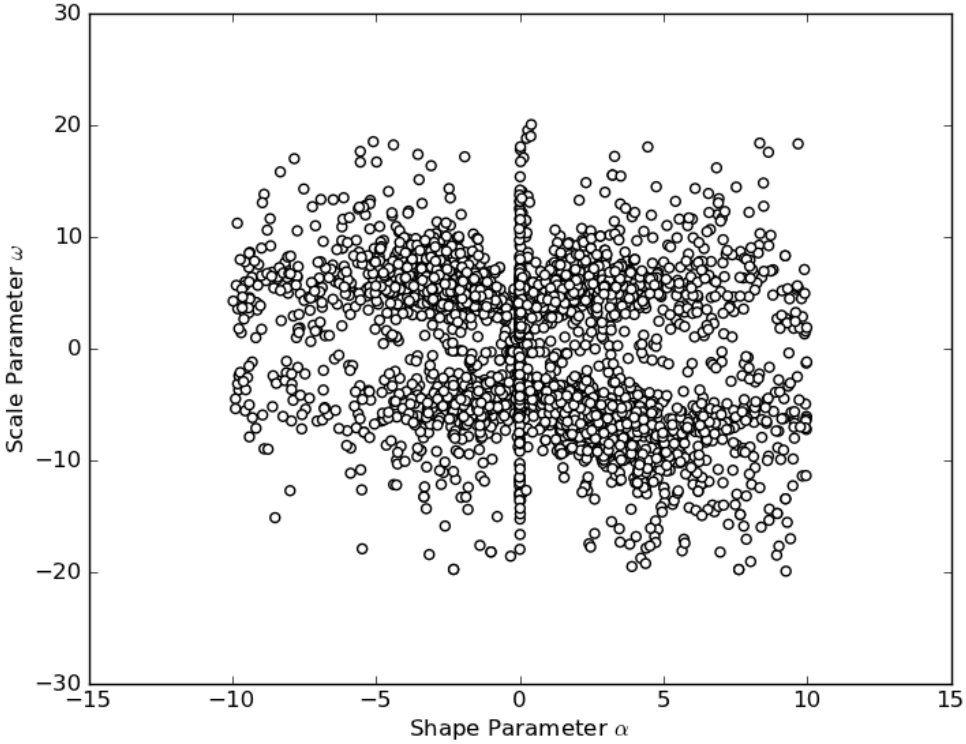

Figure 4.3: A scatterplot of the shape and scale parameters for the total [O III] sample.

* E-mail: dsgross@ucsd.edu

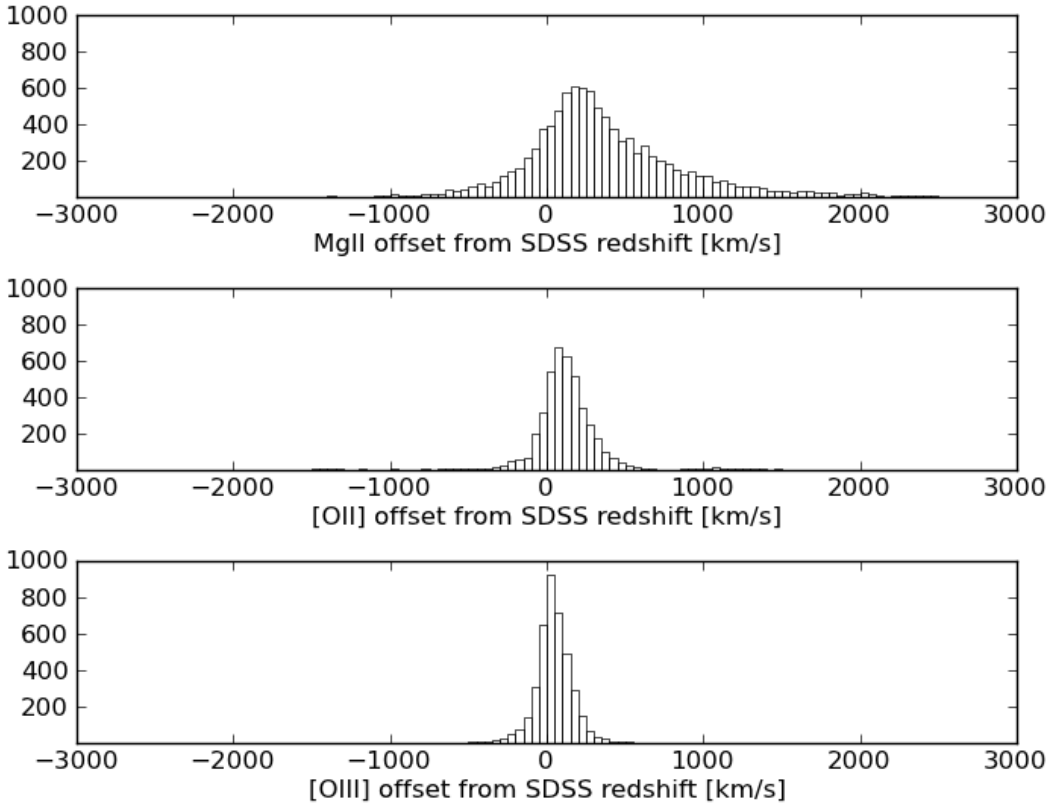

Figure 5: Velocity shifts from the reported SDSS redshift value. Each histogram is binned constant 50 km/s.

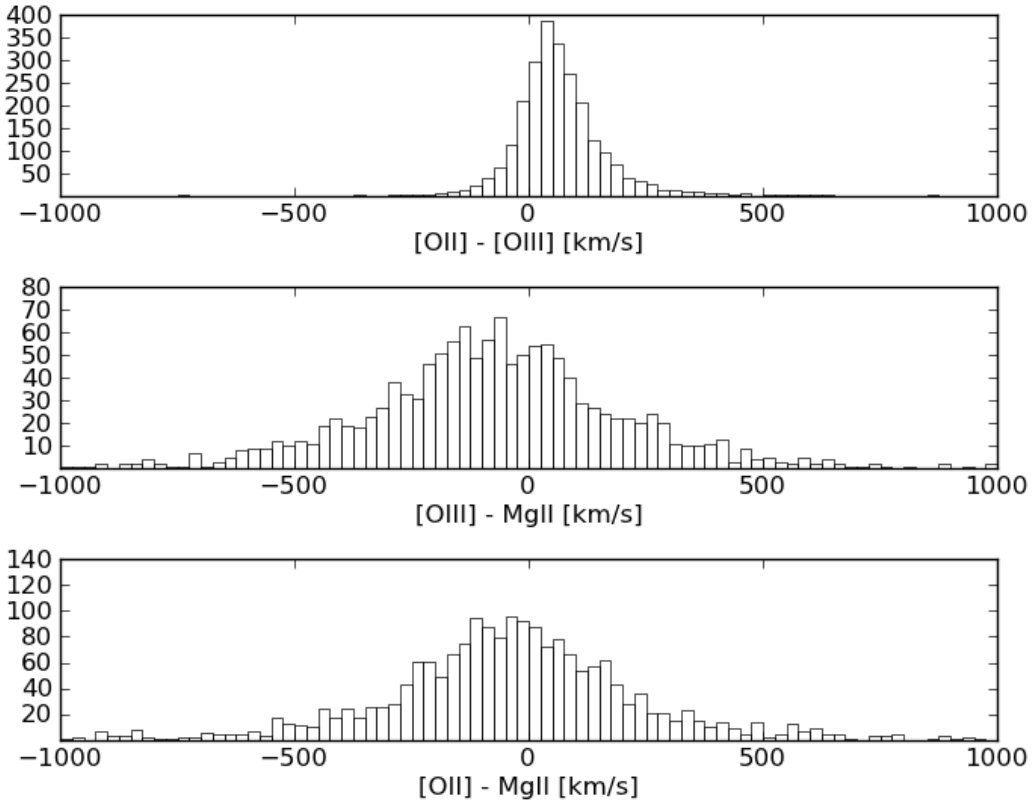

Figure 6: Velocity shifts for the line combinations in question. Each histogram is binned constant 25 km/s.